



Computational homogenization of liquid-phase sintering with seamless transition from macroscopic compressibility to incompressibility



Mikael Öhman*, Fredrik Larsson, Kenneth Runesson

Department of Applied Mechanics, Chalmers University of Technology, Hörsalsv. 7B, SE-412 96 Göteborg, Sweden

ARTICLE INFO

Article history:

Received 17 August 2012
Received in revised form 8 July 2013
Accepted 9 July 2013
Available online 20 July 2013

Keywords:

Sintering
FE²
Multiscale
Stokes' flow
Surface tension

ABSTRACT

Liquid phase sintering of particle agglomerates is modeled on the mesoscale as the viscous deformation of particle–particle contact, whereby the single driving force is the surface tension on the particle/pore interface. On the macroscale, a quasistatic equilibrium problem allows for the prediction of the shrinkage of the sintering body. The present paper presents a novel FE² formulation of the two-scale sintering problem allowing for the transition to zero porosity, implying macroscale incompressibility. The seamless transition from compressibility to incompressibility on the macroscale is accomplished by introducing a mixed variational format. This has consequences also for the formulation of the mesoscale problem, that is complemented with an extra constraint equation regarding the prolongation of the volumetric part of the macroscopic rate-of-deformation. The numerical examples shows the sintering of a single representative volume element (RVE) which is sheared beyond the point where the porosity vanishes while subjected to zero macroscopic pressure.

© 2013 The Authors. Published by Elsevier B.V. Open access under [CC BY license](http://creativecommons.org/licenses/by/3.0/).

1. Introduction

Powder metallurgy is a versatile technology for the manufacturing of components to (near) net-shape with high product quality. For a hardmetal (such as WC-Co) cold compaction of the powder to a “green body” is followed by liquid-phase sintering from the subsequent heating. This means that the binder metal Co is heated to melt in order to obtain sufficient mobility via capillary action, i.e., via surface traction, stemming from stored surface energy. The resulting flow causes gradual filling of the pore space and brings about a macroscopic shrinkage of the particle compact until a completely dense state is obtained, at least ideally. To model and quantitatively simulate the sintering process is a challenging task. The goal is to (i) estimate the final resulting quality (i.e., in terms of porosity) and (ii) to predict the final net shape and size of the sintered component.

A wealth of literature has been devoted to the modeling and simulation of the sintering process. From a mesoscale viewpoint, a classical approach is to consider so-called “unit problems”, whereby the constitutive modeling is based on diffusion and, most importantly, flow models. Among the early attempts to numerically simulate the surface-tension driven reshaping of contacting particles are those by Jagota and Dawson [1,2] and van de Vorst

[3]. In a series of papers, [4,5] emphasize efficient finite element algorithms to trace the complex 3-dimensional flow of multi-particle interaction. The main challenges are the complex subscale geometry and the moving free boundary giving rise to very large deformations and severe topology changes. Recent developments of free-boundary tracing FE-strategies for large deformations (without severe topological changes) are discussed by Dettmer and Perić [6] and Saksono and Perić [7,8]. All the mentioned work consider surface tension effects in fluids. A recent extension to include surface tension in the context of solid modeling, where anisotropic surface energy may be present, is due to [9,10].

Attempts have also been made in the literature to use macroscopic models based on nonlinear viscoelasticity and viscoplasticity. In such models the densification process is driven by the “sintering stress”, which is the macroscale manifestation of the stored surface energy. From a thermodynamical viewpoint, it is the dissipative stress that is conjugated to the current macroscale porosity, e.g., [11,12]. Among the literature on macroscale modeling, we mention [13–15].

Since computational homogenization has proven useful in a wide variety of applications, e.g., [16–20], it is natural to exploit this technique even for the present type of complex deformation process. In a previous paper, Öhman et al. [21], liquid phase sintering of particle agglomerates was modeled on the mesoscale as the viscous deformation of particle–particle contact. A FE²-strategy was outlined; however, the variational setting was applicable only under the restriction of non-vanishing macroscopic porosity (corresponding to a not fully dense end-product). The present paper

* Corresponding author. Tel.: +46 (0) 31 772 1301; fax: +46 (0) 31 772 3827.
E-mail address: mikael.ohman@chalmers.se (M. Öhman).

generalizes this situation such that it allows for the transition to zero porosity, which is accomplished by introducing a mixed variational format of the macroscale problem. We (still) assume that the particles are homogeneous and deform as a viscous fluid with sufficiently high viscosity to motivate the neglect of all acceleration terms. Moreover, the simplifying assumption is introduced that the flow properties are unaffected by temperature changes, i.e. the sintering process is only modeled during the fully heated part of the process.

The paper is structured as follows: The various features of subscale modeling (surface tension, particle arrangements within the RVE, etc.) are briefly summarized in Section 2. This is followed in Section 3 which describes the transition to macroscale and RVE problems through computational homogenization. Numerical examples, based on a single RVE, are presented in Section 5. Conclusions and an outlook to future developments are given in the final section.

2. Subscale modeling

2.1. Preliminaries

We consider a sintering body with current macroscale configuration $\Omega(t)$ in space for any given time $t \geq 0$. The boundary of $\Omega(t)$ is denoted $\partial\Omega(t)$, and we adopt standard Dirichlet and Neumann boundary conditions on the (external) boundary parts $\partial\Omega_D$ and $\partial\Omega_N$, respectively. In particular, no prescribed tractions is considered, as is the case in free sintering. Our aim is to exploit the concept of computational homogenization in order to determine the unknown $\Omega(t)$ and certain mechanical fields on $\Omega(t)$, such as the current macroscale velocity field, \mathbf{v} , the macroscale true stress field, $\bar{\boldsymbol{\sigma}}$, and the macroscale porosity field, $\bar{\phi}$ (which is the ratio of pore volume and bulk volume). We note that the initial configuration $\Omega(0)$ represents the so called “green body”, obtained after cold compaction and characterized by the inhomogeneous (macroscopic) porosity $\bar{\phi}_0$. In the case of “free sintering”, i.e., sintering without any external loading, it is clear that $\bar{\boldsymbol{\sigma}}$ represents the macroscopic residual stresses at every instant in time.

Subsequently, we shall adopt modeling on the subscale in terms of an Eulerian description of the motion, which means that it will be possible to trace the development of the current macroscale configuration $\Omega(t)$ by computing the macroscale velocity field $\mathbf{v}(\mathbf{x}, t)$ for $(\mathbf{x}, t) \in \Omega \times (0, T)$.

In a 3D representation of the microstructure the assembly of sintering particles create an open pore system (at least initially). With reasonable accuracy one may then assume that the pore surfaces are “free” surfaces, i.e., the pore gas does not impose any resistance on the motion. The situation is, of course, different in the (physically unrealistic) case of a 2D representation of the microstructure. However, in this paper, gas flow and pore pressure from trapped gas is not taken into account. In any case the pertinent surfaces associated with surface tension are particle/pore and particle/particle (contact) surfaces, as indicated in Fig. 1.

2.2. Surface tension

The “surface tension” along particle/particle and particle/pore interfaces (the latter denoted pore boundaries) is considered to be the sole “driving force” of the sintering process, and it is defined in terms of a “surface tension force” acting in the tangent plane of the surface. In the simplest (and most common) case of isotropic surface tension, this traction is characterized by the constant surface-specific surface energy γ_s in the current configuration as the single material parameter. Although we adopt this simplified model below in the numerical results, it is possible to consider the

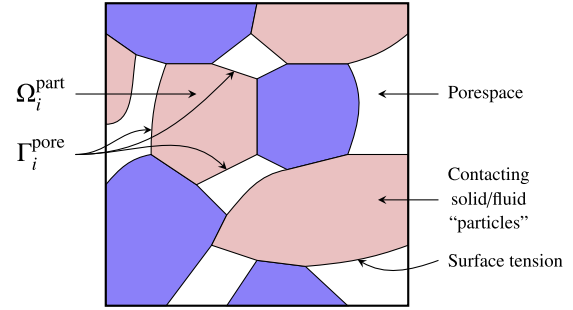


Fig. 1. Microstructure of porous particulate material with sintering particles in contact. The sintering body is subjected to Dirichlet and Neumann boundary conditions on the external boundary.

more general situation of anisotropic “surface stress” that may also depend on the surface deformation via a suitable constitutive assumption, cf. [22].

As shown in, e.g., Öhman et al. [21], it is possible to represent the surface tension force by an equivalent surface traction, henceforth denoted \mathbf{t}_s , acting on the surface (or interface). In the presently assumed case of isotropic surface tension, \mathbf{t}_s is directed in the normal direction to the surface and is given as

$$\mathbf{t}_s \stackrel{\text{def}}{=} -\kappa\gamma_s \mathbf{n}, \quad (1)$$

where $\kappa \stackrel{\text{def}}{=} -\mathbf{n} \cdot \hat{\nabla}$ is the curvature. Here, \mathbf{n} is the taken positive outwards from a convex surface, whereas $\hat{\nabla} \stackrel{\text{def}}{=} \nabla - [\nabla \cdot \mathbf{n}]\mathbf{n}$ is the surface gradient operator.

2.3. Incompressible viscous flow of the Stokes' type

We shall adopt a model for the subscale deformation within the solid particles undergoing the time-dependent sintering process. The model is simplified in the sense that elastic deformation is neglected a priori. This is a common and reasonable simplification for free sintering since the plastic deformation is dominant. It is then possible to consider a viscoplastic (fluid-like) material with intrinsic incompressibility (within the particles). Such incompressibility is expressed as $\mathbf{v} \cdot \nabla = 0$ and, hence, $\mathbf{d}_{\text{dev}} \stackrel{\text{def}}{=} [\mathbf{v} \otimes \nabla]^{\text{sym}}$. An isotropic and associated viscoplastic flow rule of the classical Perzyna type is proposed as follows:

$$\mathbf{d}_{\text{dev}} = \frac{1}{2\mu} \boldsymbol{\sigma}_{\text{dev}} + \mathbf{d}_{\text{dev}}^p(\boldsymbol{\sigma}_{\text{dev}}), \quad \mathbf{d}_{\text{dev}}^p = \frac{1}{t_*} \eta(\Phi(\sigma_e)) \frac{d\Phi}{d\boldsymbol{\sigma}}, \quad (2)$$

where t_* is the relaxation time, $\eta(\Phi)$ is an overstress function, $\Phi(\sigma_e)$ is the quasistatic yield function and $\sigma_e = \sqrt{\frac{3}{2}}|\boldsymbol{\sigma}_{\text{dev}}|$ is the equivalent stress. Upon introducing the abbreviated notation $k = \frac{\eta}{t_*} \frac{d\Phi}{d\sigma_e}$, we may solve for σ_e in terms of the equivalent rate of deformation $d_e \stackrel{\text{def}}{=} \sqrt{\frac{2}{3}}|\mathbf{d}_{\text{dev}}|$ from the equation

$$\frac{1}{3\mu} \sigma_e + k(\sigma_e) = d_e \quad (3)$$

and we, finally, obtain the “Newtonian-like” constitutive relation

$$\boldsymbol{\sigma}_{\text{dev}}(\mathbf{d}) = 2\tilde{\mu}\mathbf{d}_{\text{dev}}, \quad \tilde{\mu} \stackrel{\text{def}}{=} \frac{\sigma_e}{3d_e}. \quad (4)$$

The corresponding tangent stiffness $\mathbf{E}_{T,\text{dev}}$ in the relation $d\boldsymbol{\sigma}_{\text{dev}} = \mathbf{E}_{T,\text{dev}} : d\mathbf{d}$ (representing the linearization of the subscale constitutive problem), is given as follows:

$$\mathbf{E}_{T,\text{dev}} = 2\tilde{\mu}\mathbf{I}_{\text{dev}} + \frac{4}{9d_e^2} \left[d_e \left[\frac{1}{3\mu} + k' \right]^{-1} - \sigma_e \right] \mathbf{d}_{\text{dev}} \otimes \mathbf{d}_{\text{dev}} \quad (5)$$

with

$$k' = \frac{1}{t_*} \left[\eta \frac{d^2 \Phi}{d\sigma_e^2} + \frac{d\eta}{d\Phi} \left[\frac{d\Phi}{d\sigma_e} \right]^2 \right]. \quad (6)$$

2.4. Balance equations – strong and weak formats

Referring to Fig. 1, we consider an arbitrarily chosen collection of particles in contact (inside Ω) that constitutes the “solid particle skeleton”. Each particle domain Ω_i^{part} has part of its boundary associated with the pore surface Γ_i^{pore} . We assume (for simplicity) that the surface tension along the contact surfaces can be ignored. We also introduce the notation $\Omega^{\text{part}} \stackrel{\text{def}}{=} \cup_i \Omega_i^{\text{part}}$ and $\Gamma^{\text{pore}} \stackrel{\text{def}}{=} \cup_i \Gamma_i^{\text{pore}}$.

In the absence of acceleration, the balance equations for the quasi-static motion of the assembly of viscoplastic particles can be established in the spatial setting as follows:

$$-\boldsymbol{\sigma} \cdot \mathbf{V} = \mathbf{0} \quad \text{in } \Omega_i^{\text{part}}, \quad i = 1, 2, \dots, \quad (7a)$$

$$\mathbf{v} \cdot \mathbf{V} = 0 \quad \text{in } \Omega_i^{\text{part}}. \quad (7b)$$

As to the boundary conditions, we note the surface tension acting on the pore boundary

$$\mathbf{t} \stackrel{\text{def}}{=} \boldsymbol{\sigma} \cdot \mathbf{n} = \mathbf{t}_s \quad \text{on } \Gamma_i^{\text{pore}}, \quad i = 1, 2, \dots, \quad (8)$$

where $\boldsymbol{\sigma}(\mathbf{d}) = \boldsymbol{\sigma}_{\text{dev}}(\mathbf{d}_{\text{dev}}) - p\mathbf{I}$ is the total Cauchy stress, and p is the pressure (Lagrangian multiplier corresponding to the incompressibility constraint). In addition, there are boundary conditions (of the Dirichlet and Neumann types) on the exterior surface $\partial\Omega^{\text{part}}$ of the considered collection of particles. For simplicity of notation, we assume here that these conditions are homogeneous.

The weak form of (7) then reads:

$$\int_{\Omega^{\text{part}}} \boldsymbol{\sigma} : [\delta \mathbf{v} \otimes \mathbf{V}] d\mathbf{v} = \int_{\Gamma^{\text{pore}}} \mathbf{t}_s \cdot \delta \mathbf{v} da = - \int_{\Gamma^{\text{pore}}} \gamma_s [\delta \mathbf{v} \cdot \hat{\mathbf{V}}] da, \quad (9a)$$

$$\int_{\Omega^{\text{part}}} [\mathbf{v} \cdot \mathbf{V}] \delta p d\mathbf{v} = 0 \quad (9b)$$

for suitable test functions $\delta \mathbf{v}$ and δp that satisfy the appropriate regularity requirements (not further elaborated in this paper). To obtain the second integral on the RHS of (9a), that represents “surface tension loading”, the surface divergence theorem was used for any smooth pore surface segment Γ_i^{pore} . It is noted that γ_s may be inhomogeneous along Γ^{pore} .

Remark. In the case that the particle/particle interfaces have significant surface energy, they can be seen as part of Γ^{pore} .

3. Computational homogenization

3.1. Representative volume element

In a 2D-representation of the mesoscale features, the appropriately chosen RVE is assumed to occupy the bulk volume $\Omega_{\square}(t)$. The RVE must obviously contain a sufficient number of particles and pores to qualify as “representative” in the classical sense; however, in order to simplify the subsequent conceptual discussion and “pave the way” for the subsequent homogenization, we consider a simple arrangement of particles within the RVE. In the very simplest case, the RVE consists of one single “unit cell” containing a single contiguous pore, which is the situation shown in Fig. 2. Multi-pore RVEs were investigated in our previous paper [21].

The current “bulk” domain of the RVE at a time $t > 0$ contains the particles and the pore space, $\Omega_{\square}(t) = \Omega_{\square}^{\text{part}}(t) \cup \Omega_{\square}^{\text{pore}}(t)$, where $\Omega_{\square}^{\text{pore}}(t)$ is the domain currently occupied by the pore, whereas $\Omega_{\square}^{\text{part}}(t)$ is occupied by the particles. This is shown schematically in Fig. 2(b). The external boundary of the RVE is $\partial\Omega_{\square}(t) \stackrel{\text{def}}{=} \Gamma_{\square}(t)$. The initial configuration of the particles within the RVE (before any deformation has taken place) is denoted $\Omega_{\square}(0)$, as shown in Fig. 2(a). The boundaries of the pore-space are collectively denoted

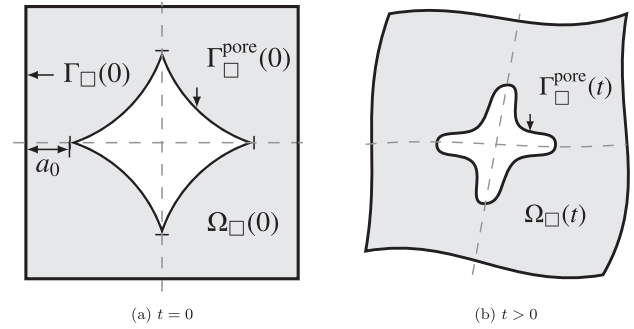


Fig. 2. (a) Initial configuration of a single-pore RVE in 2D consisting of circular particles in a perfect square lattice. The contact “points” are flattened due to precompaction. (b) Deformed configuration (sketchy).

$\Gamma_{\square}^{\text{pore}}(t)$. The boundary of the deforming particles currently contained in the RVE is then $\partial\Omega_{\square}^{\text{part}}(t) = \Gamma_{\square}(t) \cup \Gamma_{\square}^{\text{pore}}(t)$.

3.2. Homogenization – a format presuming macroscale compressibility

In the paper by Öhman et al. [21] the homogenization theory was presented in a format that is restricted to the situation that the macroscale response is compressible. In other words, the variational setting for the macroscale problem presumes non-vanishing porespace in the whole macrodomain. As soon as the porosity reaches zero in any point this format is inadequate and the algorithm breaks down, which is obviously a serious flaw. The present paper deals with this problem, and the main purpose is to show that it can be alleviated upon introducing a mixed velocity–pressure control on the macro-level. It is, therefore, relevant to first briefly summarize the theory presented in [21]:

In the most basic format it is only \mathbf{v} that is partitioned into a smooth (macroscale) part, denoted \mathbf{v}^M , and a fluctuating (subscale) part, denoted \mathbf{v}^s . In accordance with the classical assumption of first order homogenization, \mathbf{v}^M is assumed to vary linearly within the RVE, i.e.,

$$\mathbf{v}^M(\bar{\mathbf{x}}; \mathbf{x}) = \bar{\mathbf{d}}(\bar{\mathbf{x}}) \cdot [\mathbf{x} - \bar{\mathbf{x}}] \quad \text{for } \mathbf{x} \in \Omega_{\square} \quad (10)$$

or, equivalently

$$\mathbf{v}^s = 0 \quad \text{for } \mathbf{x} \in \Omega_{\square}, \quad (11)$$

i.e., a conventional Dirichlet type boundary condition on the RVEs for the momentum balance equation.

The link between $\bar{\mathbf{v}}$ and \mathbf{v}^M is established via the macroscale rate-of-deformation tensor $\bar{\mathbf{d}}$, defined as $\bar{\mathbf{d}}(\bar{\mathbf{x}}) \stackrel{\text{def}}{=} [\bar{\mathbf{v}} \otimes \mathbf{V}]^{\text{sym}}|_{\bar{\mathbf{x}}}$, where $\bar{\mathbf{v}}$ is the macroscale velocity field.

As a direct consequence of the assumption that it is only \mathbf{v} that is that is prolonged from the macro- to the subscale,¹ it is only the momentum balance that is relevant as a macroscale balance equation. Find $\bar{\mathbf{v}} \in \bar{\mathbb{V}}$ that is the solution of

$$\int_{\Omega} \bar{\boldsymbol{\sigma}}\{\bar{\mathbf{d}}\} : [\delta \bar{\mathbf{v}} \otimes \mathbf{V}] d\mathbf{v} = 0 \quad \forall \delta \bar{\mathbf{v}} \in \bar{\mathbb{V}}^0. \quad (12)$$

where the macroscale (homogenized) stress $\bar{\boldsymbol{\sigma}}$ is computed as

$$\bar{\boldsymbol{\sigma}} = \langle \boldsymbol{\sigma} \rangle_{\square} - \frac{1}{|\Omega_{\square}|} \int_{\Gamma_{\square}^{\text{pore}}} [\mathbf{t}_s \otimes [\mathbf{x} - \bar{\mathbf{x}}]]^{\text{sym}} da, \quad (13)$$

$$= \frac{1}{|\Omega_{\square}|} \int_{\Gamma_{\square}^{\text{pore}}} [\mathbf{t} \otimes [\mathbf{x} - \bar{\mathbf{x}}]]^{\text{sym}} da. \quad (14)$$

¹ Here, we refer to “prolongation” as the construction of a resolved field by a (linear) Taylor series expansion of the macroscale field on the subscale.

The volume average is defined as

$$\langle \bullet \rangle_{\square} \stackrel{\text{def}}{=} \frac{1}{|\Omega_{\square}|} \int_{\Omega_{\text{part}}} \bullet \, d\mathbf{v}, \quad (15)$$

and it must be noted that, although stresses are defined in the fluid region Ω_{part} , averaging is on the bulk volume Ω_{\square} .

The RVE-problem is formulated as follows: For given value of the macroscale variable $\bar{\mathbf{d}}$, find $(\mathbf{v}^s, \mathbf{p}) \in \mathbb{V}_{\square}^{(D)} \times \mathbb{P}_{\square}$ that solve the system

$$a_{\square}(\mathbf{v}^M + \mathbf{v}^s; \delta \mathbf{v}^s) + b_{\square}(p, \delta \mathbf{v}^s) = l_{\square}^{\text{pore}}(\delta \mathbf{v}^s) \quad \forall \delta \mathbf{v}^s \in \mathbb{V}_{\square}^{(D)}, \quad (16a)$$

$$b_{\square}(\delta p, \mathbf{v}^M + \mathbf{v}^s) = 0 \quad \forall \delta p \in \mathbb{P}_{\square}, \quad (16b)$$

where the variational forms are defined as

$$a_{\square}(\mathbf{v}; \delta \mathbf{v}) \stackrel{\text{def}}{=} \langle \boldsymbol{\sigma}_{\text{dev}}(\mathbf{d}) : [\delta \mathbf{v} \otimes \nabla] \rangle_{\square} = \frac{1}{|\Omega_{\square}|} \int_{\Omega_{\text{part}}} \boldsymbol{\sigma}_{\text{dev}}(\mathbf{d}) : [\delta \mathbf{v} \otimes \nabla] \, d\mathbf{v}, \quad (17a)$$

$$b_{\square}(p, \delta \mathbf{v}) \stackrel{\text{def}}{=} - \langle [\delta \mathbf{v} \cdot \nabla] p \rangle_{\square} = - \frac{1}{|\Omega_{\square}|} \int_{\Omega_{\text{part}}} [\delta \mathbf{v} \cdot \nabla] p \, d\mathbf{v}, \quad (17b)$$

$$l_{\square}^{\text{pore}}(\delta \mathbf{v}) \stackrel{\text{def}}{=} - \frac{1}{|\Omega_{\square}|} \int_{\Gamma_{\text{pore}}} \gamma_s [\delta \mathbf{v} \cdot \hat{\mathbf{v}}] \, da. \quad (17c)$$

Details regarding the solution of this system in terms of the relevant iteration procedure and how to compute the ATS-tensor in the FE² algorithm are given in [21] and are not further elaborated here. The flow chart is summarized in Fig. 3.

In Fig. 3, we used the split into deviatoric and volumetric parts:

$$\bar{\mathbf{d}} = \bar{\mathbf{d}}_{\text{dev}} + \frac{1}{3} \bar{e} \mathbf{I} \quad \text{where } \bar{e} \stackrel{\text{def}}{=} \bar{\mathbf{d}} : \mathbf{I}, \quad \bar{\mathbf{d}}_{\text{dev}} \stackrel{\text{def}}{=} \bar{\mathbf{d}} - \frac{1}{3} \bar{e} \mathbf{I}, \quad (18)$$

$$\bar{\boldsymbol{\sigma}} = \bar{\boldsymbol{\sigma}}_{\text{dev}} - \bar{p} \mathbf{I} \quad \text{where } \bar{p} \stackrel{\text{def}}{=} -\frac{1}{3} \bar{\boldsymbol{\sigma}} : \mathbf{I}, \quad \bar{\boldsymbol{\sigma}}_{\text{dev}} \stackrel{\text{def}}{=} \bar{\boldsymbol{\sigma}} + \bar{p} \mathbf{I}, \quad (19)$$

and where $\bar{\mathbf{d}}_{\text{dev}} = [\bar{\mathbf{v}} \otimes \nabla]_{\text{dev}}^{\text{sym}}$, $\bar{e} = \bar{\mathbf{v}} \cdot \nabla$.

Remark. The split in deviatoric and volumetric parts is never (or at least does not need to be) exploited operationally in the numerical algorithm; however, the situation is entirely different in the format discussed in the next Section. □

3.3. Homogenization – a format allowing transition from macroscale compressibility to incompressibility

In this Section we outline the strategy for replacing the velocity-based format in Section 3.2 to a mixed variational format on the macroscale. Hence, we introduce the macroscale pressure \bar{p} as an independent variable in the momentum balance equation, and

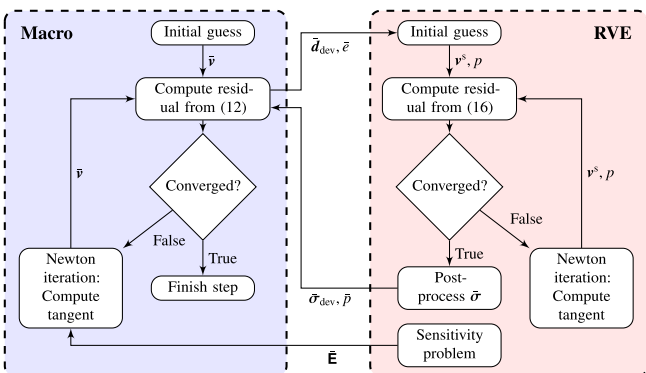


Fig. 3. Flow-chart of FE²-format valid only for macroscopic compressibility.

the relation $\bar{e} = \bar{\mathbf{v}} \cdot \nabla$ is imposed in a weak sense. The resulting macroscale problem then becomes: find $(\bar{\mathbf{v}}, \bar{p}) \in \bar{\mathbb{V}} \times \bar{\mathbb{P}}$ that solve

$$\int_{\Omega} \bar{\boldsymbol{\sigma}}_{\text{dev}}\{\bar{\mathbf{d}}_{\text{dev}}, \bar{p}\} : [\delta \bar{\mathbf{v}} \otimes \nabla] \, d\mathbf{v} + \int_{\Omega} -\bar{p} [\delta \bar{\mathbf{v}} \cdot \nabla] \, d\mathbf{v} = 0 \quad \forall \delta \bar{\mathbf{v}} \in \bar{\mathbb{V}}^0, \quad (20a)$$

$$\int_{\Omega} [\bar{e}\{\bar{\mathbf{d}}_{\text{dev}}, \bar{p}\} - \bar{\mathbf{v}} \cdot \nabla] \delta \bar{p} \, d\mathbf{v} = 0 \quad \forall \delta \bar{p} \in \bar{\mathbb{P}} \quad (20b)$$

which system of equations thus replaces (12).

The prolongation of $\bar{\mathbf{d}}$ to the RVE remains as before; however, it is useful to note that \mathbf{v}^M can be expanded as

$$\mathbf{v}^M = \mathbf{v}_{\text{dev}}^M + \mathbf{v}_{\text{vol}}^M = \bar{\mathbf{d}}_{\text{dev}} \cdot [\mathbf{x} - \bar{\mathbf{x}}] + \bar{e} \frac{1}{3} [\mathbf{x} - \bar{\mathbf{x}}]. \quad (21)$$

The important difference to the previous formulation is that the volumetric part is no longer an input but part of the solution of the RVE-problem. The corresponding complementary equation is obtained upon testing the momentum balance equation with the volumetric part of \mathbf{v}^M . As the result, we obtain the following RVE-problem: For given macroscale variables $\bar{\mathbf{d}}_{\text{dev}}$ and \bar{p} , find $(\mathbf{v}^s, p, \bar{e}) \in \mathbb{V}_{\square}^{(D)} \times \mathbb{P}_{\square} \times \mathbb{R}$ that solve the system

$$a_{\square}(\mathbf{v}_{\text{dev}}^M(\bar{\mathbf{d}}_{\text{dev}}) + \mathbf{v}^s; \delta \mathbf{v}^s) + b_{\square}(p, \delta \mathbf{v}^s) = l_{\square}^{\text{pore}}(\delta \mathbf{v}^s) \quad \forall \delta \mathbf{v}^s \in \mathbb{V}_{\square}^{(D)}, \quad (22a)$$

$$b_{\square}(\delta p, \mathbf{v}_{\text{vol}}^M(\bar{e}) + \mathbf{v}^s) = 0 \quad \forall \delta p \in \mathbb{P}_{\square}, \quad (22b)$$

$$b_{\square}(p, \mathbf{x}_m) \delta \bar{e} = [l_{\square}^{\text{pore}}(\mathbf{x}_m) - \bar{p}] \delta \bar{e} \quad \forall \delta \bar{e} \in \mathbb{R}, \quad (22c)$$

where $\mathbf{x}_m \stackrel{\text{def}}{=} \frac{1}{3} [\mathbf{x} - \bar{\mathbf{x}}]$. Detailed derivations of (22a) and (22c) are shown in Appendix A.

It is worth noting that the space of test functions for the sub-scale fluctuation fields, $\mathbb{V}_{\square}^{(D)}$, have not changed in this new formulation, and \mathbf{v}^s is still zero on the RVE boundary. Hence, Dirichlet boundary conditions are still adopted for the velocity field. Only the control variables, summarized in Fig. 4, have changed.

It turns out that the physical interpretation of (22c) is that the RVE pressure plus the surface tension contribution must equal the macroscopic pressure;

$$\langle p \rangle_{\square} + \frac{1}{|\Omega_{\square}|} \int_{\Gamma_{\text{pore}}} \frac{2}{3} \gamma_s \, da = \bar{p}. \quad (23)$$

As to the “feed-back” of variables to the macroscale problem, we note that that \bar{e} is part of the solution of the RVE-problem, whereas $\bar{\boldsymbol{\sigma}}_{\text{dev}}\{\bar{\mathbf{d}}_{\text{dev}}, \bar{p}\}$ is post-processed as

$$\bar{\boldsymbol{\sigma}}_{\text{dev}} = \frac{1}{|\Omega_{\square}|} \int_{\Gamma_{\text{pore}}} [\mathbf{t} \otimes [\mathbf{x} - \bar{\mathbf{x}}]]^{\text{sym}} \, da + \bar{p} \mathbf{I}, \quad (24)$$

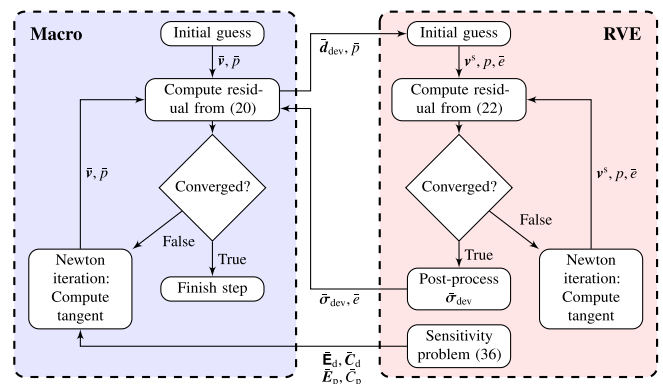


Fig. 4. Flow-chart of FE²-format for seamless transition from macroscopic compressibility to incompressibility.

Remark. It was used explicitly in (22a) that $\boldsymbol{\sigma}_{\text{dev}}$ is proportional to \mathbf{d}_{dev} . \square

3.3.1. Macroscale incompressibility

Consider the extreme situation of macroscopic incompressibility, defined by the condition $\bar{\mathbf{e}} = \mathbf{0}$. The system (20) is then simplified as follows:

$$\int_{\Omega} \bar{\boldsymbol{\sigma}}_{\text{dev}}\{\bar{\mathbf{d}}_{\text{dev}}, \bar{p}\} : [\delta \bar{\mathbf{v}} \otimes \mathbf{V}] d\mathbf{v} + \int_{\Omega} -\bar{p} [\delta \bar{\mathbf{v}} \cdot \mathbf{V}] d\mathbf{v} = 0 \quad \forall \delta \bar{\mathbf{v}} \in \bar{\mathbb{V}}^0, \quad (25a)$$

$$\int_{\Omega} \bar{\mathbf{v}} \cdot \mathbf{V} \delta \bar{p} d\mathbf{v} \quad \forall \delta \bar{p} \in \bar{\mathbb{P}}, \quad (25b)$$

i.e., \bar{p} is now a classical Lagrange multiplier. Moreover, the result $\bar{\mathbf{e}} = \mathbf{0}$ is obtained as part of the solution of the simplified RVE-problem (22) from setting $\mathbb{I}_{\square}^{\text{pore}}(\delta \mathbf{v}^s) = \mathbf{0}$:

$$a_{\square}(\mathbf{v}_{\text{dev}}^M(\bar{\mathbf{d}}_{\text{dev}}) + \mathbf{v}^s; \delta \mathbf{v}^s) + b_{\square}(p, \delta \mathbf{v}^s) = 0 \quad \forall \delta \mathbf{v}^s \in \mathbb{V}_{\square}^{(D)}, \quad (26a)$$

$$b_{\square}(\delta p, \mathbf{v}_{\text{vol}}^M(\bar{\mathbf{e}}) + \mathbf{v}^s) = 0 \quad \forall \delta p \in \mathbb{P}_{\square}, \quad (26b)$$

$$b_{\square}(p, \mathbf{x}_m) \delta \bar{\mathbf{e}} = -\bar{p} \delta \bar{\mathbf{e}} \quad \forall \delta \bar{\mathbf{e}} \in \mathbb{R}. \quad (26c)$$

More precisely, $\bar{\mathbf{e}} = \mathbf{0}$ is obtained as the solution of (26b) upon choosing $\delta p = 1$. Furthermore (26c) guarantees a unique solution \mathbf{v}^s, p for the incompressible Stokes' problem by omitting the otherwise arbitrary constant in p .

We thus remark that the problem format employed in (20) does indeed represent both the macroscopically compressible and incompressible states such that the transition between them is seamless.

3.4. Iterative solution of RVE-problem using Newton's method

The RVE-problem (22) must be solved iteratively in practice due to the subscale nonlinearities. To this end, we first rewrite the RVE-problem as the vanishing residuals

$$R_{\square}^v(\mathbf{v}^s, p; \delta \mathbf{v}^s) \stackrel{\text{def}}{=} \mathbb{I}_{\square}^{\text{pore}}(\delta \mathbf{v}^s) - a_{\square}(\mathbf{v}_{\text{dev}}^M(\bar{\mathbf{d}}_{\text{dev}}) + \mathbf{v}^s; \delta \mathbf{v}^s) - b_{\square}(p, \delta \mathbf{v}^s) \quad \forall \delta \mathbf{v}^s \in \mathbb{V}_{\square}^{(D)}, \quad (27a)$$

$$R_{\square}^p(\bar{\mathbf{e}}, \mathbf{v}^s; \delta p) \stackrel{\text{def}}{=} -b_{\square}(\delta p, \mathbf{v}_{\text{vol}}^M(\bar{\mathbf{e}}) + \mathbf{v}^s) \quad \forall \delta p \in \mathbb{P}_{\square}, \quad (27b)$$

$$R_{\square}^d(p; \delta \bar{\mathbf{e}}) \stackrel{\text{def}}{=} [\mathbb{I}_{\square}^{\text{pore}}(\mathbf{x}_m) = \bar{p} - b_{\square}(p, \mathbf{x}_m)] \delta \bar{\mathbf{e}} \quad \forall \delta \bar{\mathbf{e}} \in \mathbb{R}. \quad (27c)$$

Newton's iteration method for finding the unknown variables $\mathbf{v}^s, p, \bar{\mathbf{e}}$ for given $\bar{\mathbf{d}}_{\text{dev}}$ and \bar{p} then becomes: For $k = 1, 2, \dots$, compute $\mathbf{v}^{s(k+1)} = \mathbf{v}^{s(k)} + \Delta \mathbf{v}^s$, $p^{(k+1)} = p^{(k)} + \Delta p$, $\bar{\mathbf{e}}^{(k+1)} = \bar{\mathbf{e}}^{(k)} + \Delta \bar{\mathbf{e}}$, (28)

where the iterative updates $\Delta \mathbf{v}^s \in \mathbb{V}_{\square}^{(D)}$, $\Delta p \in \mathbb{P}_{\square}$, $\Delta \bar{\mathbf{e}} \in \mathbb{R}$ are solved from the tangent equations

$$(a_{\square})'(\mathbf{v}_{\text{dev}}^M + \mathbf{v}^{s(k)}; \delta \mathbf{v}^s, \Delta \mathbf{v}^s) + b_{\square}(\Delta p, \delta \mathbf{v}^s) = R_{\square}^v(\bullet^{(k)}; \delta \mathbf{v}^s) \quad \forall \delta \mathbf{v}^s \in \mathbb{V}_{\square}^{(D)}, \quad (29a)$$

$$b_{\square}(\delta p, \mathbf{v}_{\text{vol}}^M(\Delta \bar{\mathbf{e}}) + \Delta \mathbf{v}^s) = R_{\square}^p(\bullet^{(k)}; \delta p) \quad \forall \delta p \in \mathbb{P}_{\square}, \quad (29b)$$

$$b_{\square}(\Delta p, \mathbf{x}_m) \delta \bar{\mathbf{e}} = R_{\square}^d(\bullet^{(k)}; \delta \bar{\mathbf{e}}) \quad \forall \delta \bar{\mathbf{e}} \in \mathbb{R} \quad (29c)$$

until the residuals are sufficiently small. The tangent form $(a_{\square})'$ is given explicitly as

$$(a_{\square})'(\bullet; \delta \mathbf{v}^s, \Delta \mathbf{v}^s) = \langle [\delta \mathbf{v} \otimes \mathbf{V}] : \mathbf{E}_{\text{T,dev}}(\bullet) : [\Delta \mathbf{v}^s \otimes \mathbf{V}] \rangle_{\square}, \quad (30)$$

where the tangent $\mathbf{E}_{\text{T,dev}}$ is defined in (5).

4. Mixed macroscale problem format – selected issues

4.1. Macroscale problem – abstract format

The macroscale problem in (20) can be put in the more abstract form as follows: find $(\bar{\mathbf{v}}, \bar{p}) \in \bar{\mathbb{V}} \times \bar{\mathbb{P}}$ that solve

$$\bar{a}\{\bar{\mathbf{v}}, \bar{p}; \delta \bar{\mathbf{v}}\} + \bar{b}\{\bar{p}, \delta \bar{\mathbf{v}}\} = 0 \quad \forall \delta \bar{\mathbf{v}} \in \bar{\mathbb{V}}^0, \quad (31a)$$

$$\bar{b}\{\delta \bar{p}, \bar{\mathbf{v}}\} + \bar{c}\{\bar{\mathbf{v}}, \bar{p}; \delta \bar{p}\} = 0 \quad \forall \delta \bar{p} \in \bar{\mathbb{P}}, \quad (31b)$$

where the pertinent variational forms are given as

$$\bar{a}\{\bar{\mathbf{v}}, \bar{p}; \delta \bar{\mathbf{v}}\} \stackrel{\text{def}}{=} \int_{\Omega} \bar{\boldsymbol{\sigma}}_{\text{dev}}\{[\bar{\mathbf{v}} \otimes \mathbf{V}]_{\text{dev}}^{\text{sym}}, \bar{p}\} : [\delta \bar{\mathbf{v}} \otimes \mathbf{V}]_{\text{dev}}^{\text{sym}} d\mathbf{v}, \quad (32)$$

$$\bar{b}\{\bar{p}, \delta \bar{\mathbf{v}}\} \stackrel{\text{def}}{=} - \int_{\Omega} \bar{p} [\delta \bar{\mathbf{v}} \cdot \mathbf{V}] d\mathbf{v}, \quad (33)$$

$$\bar{c}\{\bar{\mathbf{v}}, \bar{p}; \delta \bar{p}\} \stackrel{\text{def}}{=} \int_{\Omega} \bar{\mathbf{e}}\{[\bar{\mathbf{v}} \otimes \mathbf{V}]_{\text{dev}}^{\text{sym}}, \bar{p}\} \delta \bar{p} d\mathbf{v}. \quad (34)$$

Newton iterations for solving the system (31) employ the algorithmic tangents

$$d\bar{\boldsymbol{\sigma}}_{\text{dev}} = \bar{\mathbf{E}}_d : d\bar{\mathbf{d}}_{\text{dev}} + \bar{\mathbf{E}}_p d\bar{p}, \quad (35a)$$

$$d\bar{\mathbf{e}} = \bar{\mathbf{C}}_d : d\bar{\mathbf{d}}_{\text{dev}} + \bar{\mathbf{C}}_p d\bar{p} \quad (35b)$$

taken with respect to $\bar{\mathbf{d}}_{\text{dev}} \stackrel{\text{def}}{=} [\bar{\mathbf{v}} \otimes \mathbf{V}]_{\text{dev}}^{\text{sym}}$ and \bar{p} , such that the increments $\Delta \bar{\mathbf{v}}$ and $\Delta \bar{p}$ are obtained from the macroscale tangent problem

$$\bar{a}'_v\{\bullet; \delta \bar{\mathbf{v}}, \Delta \bar{\mathbf{v}}\} + \bar{a}'_p\{\bullet; \delta \bar{\mathbf{v}}, \Delta \bar{p}\} + \bar{b}\{\Delta \bar{p}, \delta \bar{\mathbf{v}}\} = -\bar{a}\{\bullet; \delta \bar{\mathbf{v}}\} - \bar{b}\{\bullet, \delta \bar{\mathbf{v}}\} \quad \forall \delta \bar{\mathbf{v}} \in \bar{\mathbb{V}}^0, \quad (36a)$$

$$\bar{b}'\{\delta \bar{p}, \Delta \bar{\mathbf{v}}\} + \bar{c}'_v\{\bullet; \delta \bar{p}, \Delta \bar{\mathbf{v}}\} + \bar{c}'_p\{\bullet; \delta \bar{p}, \Delta \bar{p}\} = -\bar{b}\{\delta \bar{p}, \bullet\} - \bar{c}\{\bullet, \delta \bar{p}\} \quad \forall \delta \bar{p} \in \bar{\mathbb{P}}, \quad (36b)$$

where

$$\bar{a}'_v\{\bullet; \delta \bar{\mathbf{v}}, \Delta \bar{\mathbf{v}}\} \int_{\Omega} [\delta \bar{\mathbf{v}} \otimes \mathbf{V}]_{\text{dev}}^{\text{sym}} : \bar{\mathbf{E}}_d : [\Delta \bar{\mathbf{v}} \otimes \mathbf{V}]_{\text{dev}}^{\text{sym}} d\mathbf{v}, \quad (37)$$

$$\bar{a}'_p\{\bullet; \delta \bar{\mathbf{v}}, \Delta \bar{p}\} = \int_{\Omega} [\delta \bar{\mathbf{v}} \otimes \mathbf{V}]_{\text{dev}}^{\text{sym}} : \bar{\mathbf{E}}_p \Delta \bar{p} d\mathbf{v}, \quad (38)$$

$$\bar{c}'_v\{\bullet; \delta \bar{p}, \Delta \bar{\mathbf{v}}\} = \int_{\Omega} \delta \bar{p} \bar{\mathbf{C}}_d : [\Delta \bar{\mathbf{v}} \otimes \mathbf{V}]_{\text{dev}}^{\text{sym}} d\mathbf{v}, \quad (39)$$

$$\bar{c}'_p\{\bullet; \delta \bar{p}, \Delta \bar{p}\} = \int_{\Omega} \delta \bar{p} \bar{\mathbf{C}}_p \Delta \bar{p} d\mathbf{v}. \quad (40)$$

4.2. Computation of macroscale algorithmic tangent tensors

The algorithmic tensors $\bar{\mathbf{E}}_d, \bar{\mathbf{E}}_p, \bar{\mathbf{C}}_d$ and $\bar{\mathbf{C}}_p$, needed in order to carry out macroscale Newton iterations in (36), are obtained for perturbations of the RVE-solution expressed in terms of perturbations of $\bar{\mathbf{d}}_{\text{dev}}$ and \bar{p} . However, in order to obtain a suitable representation of deviatoric macroscale 2nd order tensors, we conclude that it is convenient to replace the standard dyad bases with a complete, orthonormal, basis $\{\mathbf{E}_i\}_{i=1}^{n_b}$ for symmetric deviatoric tensors. Hence, these base dyadics satisfy the conditions $\mathbf{E}_i : \mathbf{E}_j = \delta_{ij}$ and $\mathbf{E}_i : \mathbf{I} = 0$. Examples of such bases are shown in the Appendix. We may now adopt the expansions

$$\bar{\mathbf{d}}_{\text{dev}} = \sum_i^{n_B} \bar{\mathbf{d}}_{\text{dev},i} \mathbf{E}_i, \quad \bar{\mathbf{d}}_{\text{dev},i} = \bar{\mathbf{d}}_{\text{dev}} : \mathbf{E}_i, \quad (41)$$

$$\bar{\boldsymbol{\sigma}}_{\text{dev}} = \sum_i^{n_B} \bar{\boldsymbol{\sigma}}_{\text{dev},i} \mathbf{E}_i, \quad \bar{\boldsymbol{\sigma}}_{\text{dev},i} = \bar{\boldsymbol{\sigma}}_{\text{dev}} : \mathbf{E}_i. \quad (42)$$

Remark. For 3D $n_B = 5$, while for 2D $n_B = 2$.

We are now in the position to compute *sensitivity fields*, corresponding to a unit variation of the macroscale variables $\bar{\mathbf{d}}_{\text{dev},i}$ and \bar{p} . First, we shall need to compute the differentials

$$d\mathbf{v} = d\mathbf{v}_{\text{dev}}^M + d\mathbf{v}_{\text{vol}}^M + d\mathbf{v}^s. \quad (43)$$

Using (41) we obtain

$$d\mathbf{v}_{\text{dev}}^M = \sum_i \hat{\mathbf{v}}_{\text{dev}}^{M(i)} d\bar{\mathbf{d}}_{\text{dev},i}, \quad \hat{\mathbf{v}}_{\text{dev}}^{M(i)} = \mathbf{E}_i \cdot [\mathbf{x} - \bar{\mathbf{x}}], \quad (44)$$

where $\hat{\mathbf{v}}_{\text{dev}}^{M(i)}$ are the “unit velocity fields”. In analogy with the definition of $\hat{\mathbf{v}}_{\text{dev}}^{M(i)}$ in (44), we introduce the “unit fields”, or sensitivities, due to a unit perturbation of the components $d\bar{\mathbf{d}}_{\text{dev},i}$ and of $d\bar{p}$, via the *ansatz*

$$d\mathbf{v}_{\text{vol}}^M = \mathbf{x}_m d\bar{e} \quad \text{with} \quad d\bar{e} = \sum_i \hat{e}_d^{(i)} d\bar{\mathbf{d}}_{\text{dev},i} + \hat{e}_p d\bar{p}, \quad (45)$$

$$d\mathbf{v}^s = \sum_i \hat{\mathbf{v}}_d^{s(i)} d\bar{\mathbf{d}}_{\text{dev},i} + \hat{\mathbf{v}}_p^s d\bar{p}, \quad (46)$$

$$dp = \sum_i \hat{p}_d^{(i)} d\bar{\mathbf{d}}_{\text{dev},i} + \hat{p}_p d\bar{p}. \quad (47)$$

Upon using the identity $\bar{\boldsymbol{\sigma}} = \frac{1}{|\Omega_\square|} \int_{\Gamma_\square} \mathbf{t} \otimes [\mathbf{x} - \bar{\mathbf{x}}] da$, we deduce the component representation

$$\begin{aligned} d\bar{\boldsymbol{\sigma}}_{\text{dev},i} &= d\bar{\boldsymbol{\sigma}} : \mathbf{E}_i = d \left[\frac{1}{|\Omega_\square|} \int_{\Gamma_\square} \mathbf{t} \cdot \mathbf{E}_i \cdot [\mathbf{x} - \bar{\mathbf{x}}] da \right] \\ &= -d \left[R_\square^V(\bullet; \hat{\mathbf{v}}_{\text{dev}}^{M(i)}) \right] \\ &= d \left[a_\square(\bullet; \hat{\mathbf{v}}_{\text{dev}}^{M(i)}) \right] + d \left[b_\square(\bullet; \hat{\mathbf{v}}_{\text{dev}}^{M(i)}) \right] - d \left[p_\square^{\text{pore}}(\hat{\mathbf{v}}_{\text{dev}}^{M(i)}) \right] \\ &= (a_\square)'(\bullet; \hat{\mathbf{v}}_{\text{dev}}^{M(i)}, d\mathbf{v}) \\ &= \sum_j \underbrace{(a_\square)'(\bullet; \hat{\mathbf{v}}_{\text{dev}}^{M(i)}, \hat{\mathbf{v}}_{\text{dev}}^{M(j)} + \hat{\mathbf{v}}_d^{s(j)})}_{\frac{\partial \bar{\boldsymbol{\sigma}}_{\text{dev},i}}{\partial \bar{\mathbf{d}}_{\text{dev},j}}} d\bar{\mathbf{d}}_{\text{dev},j} \\ &\quad + \underbrace{(a_\square)'(\bullet; \hat{\mathbf{v}}_{\text{dev}}^{M(i)}, \hat{\mathbf{v}}_p^s)}_{\frac{\partial \bar{\boldsymbol{\sigma}}_{\text{dev},i}}{\partial \bar{p}}} d\bar{p}, \end{aligned} \quad (48)$$

where we used that $b_\square(\bullet; \hat{\mathbf{v}}_{\text{dev}}^{M(i)}) = 0$ and $d \left[p_\square^{\text{pore}}(\hat{\mathbf{v}}_{\text{dev}}^{M(i)}) \right] = 0$. Hence, the (symbolic) tensor format of (48) is obtained from

$$\begin{aligned} d\bar{\boldsymbol{\sigma}}_{\text{dev}} &= \sum_i \mathbf{E}_i d\bar{\boldsymbol{\sigma}}_{\text{dev},i} = \sum_{ij} \mathbf{E}_i \frac{\partial \bar{\boldsymbol{\sigma}}_{\text{dev},i}}{\partial \bar{\mathbf{d}}_{\text{dev},j}} d\bar{\mathbf{d}}_{\text{dev},j} + \sum_i \mathbf{E}_i \frac{\partial \bar{\boldsymbol{\sigma}}_{\text{dev},i}}{\partial \bar{p}} d\bar{p} \\ &= \sum_{ij} \mathbf{E}_i \frac{\partial \bar{\boldsymbol{\sigma}}_{\text{dev},i}}{\partial \bar{\mathbf{d}}_{\text{dev},j}} [\mathbf{E}_j : d\bar{\mathbf{d}}_{\text{dev}}] + \sum_i \mathbf{E}_i \frac{\partial \bar{\boldsymbol{\sigma}}_{\text{dev},i}}{\partial \bar{p}} d\bar{p} \\ &= \underbrace{\left[\sum_{ij} \frac{\partial \bar{\boldsymbol{\sigma}}_{\text{dev},i}}{\partial \bar{\mathbf{d}}_{\text{dev},j}} \mathbf{E}_i \otimes \mathbf{E}_j \right]}_{\mathbf{E}_d} : d\bar{\mathbf{d}}_{\text{dev}} + \underbrace{\sum_i \frac{\partial \bar{\boldsymbol{\sigma}}_{\text{dev},i}}{\partial \bar{p}} \mathbf{E}_i}_{\bar{\mathbf{E}}_p} d\bar{p}. \end{aligned} \quad (49)$$

We also obtain trivially the relation

$$d\bar{e} = \sum_i \hat{e}_d^{(i)} d\bar{\mathbf{d}}_{\text{dev},i} + \hat{e}_p d\bar{p} = \underbrace{\left[\sum_i \hat{e}_d^{(i)} \mathbf{E}_i \right]}_{\bar{\mathbf{C}}_d} : d\bar{\mathbf{d}}_{\text{dev}} + \underbrace{\hat{e}_p}_{\bar{\mathbf{C}}_p} d\bar{p}. \quad (50)$$

In order to compute the pertinent sensitivities, we conclude that the state Eqs. (22) must hold for $\bar{\mathbf{d}}_{\text{dev}}, \bar{p}$ as well as for a perturbed state $\bar{\mathbf{d}}_{\text{dev}} + d\bar{\mathbf{d}}_{\text{dev}}, \bar{p} + d\bar{p}$. These perturbations give rise to perturbations of $d\mathbf{v}^s \in \mathbb{V}_\square^{(D)}$, $d\mathbf{p} \in \mathbb{P}_\square$ and of $d\bar{e} \in \mathbb{R}$ (that defines $d\mathbf{v}_{\text{vol}}^M$). Using the linearized form (29) at equilibrium with the split in (43), we obtain the appropriate tangent problem:

$$(a_\square)'(\bullet; \delta\mathbf{v}^s, d\mathbf{v}_{\text{dev}}^M + d\mathbf{v}^s) + b_\square(d\mathbf{p}, \delta\mathbf{v}^s) = 0 \quad \forall \delta\mathbf{v}^s \in \mathbb{V}_\square^{(D)}, \quad (51a)$$

$$b_\square(\delta p, d\mathbf{v}_{\text{vol}}^M + d\mathbf{v}^s) = 0 \quad \forall \delta p \in \mathbb{P}_\square, \quad (51b)$$

$$b_\square(d\mathbf{p}, \mathbf{x}_m) \delta \bar{e} = -d\bar{p} \delta \bar{e} \quad \forall \delta \bar{e} \in \mathbb{R} \quad (51c)$$

which must hold for any given $d\bar{\mathbf{d}}_{\text{dev}}$ and $d\bar{p}$. We thus consider the cases $(d\bar{\mathbf{d}}_{\text{dev}} \neq \mathbf{0}, d\bar{p} = 0)$ and $(d\bar{\mathbf{d}}_{\text{dev}} = \mathbf{0}, d\bar{p} \neq 0)$ in turn:

1. $d\bar{\mathbf{d}}_{\text{dev}} = \mathbf{E}_i$ ($\bar{\mathbf{d}}_{\text{dev},i} = 1, \bar{\mathbf{d}}_{\text{dev},j} = 0$ for $j \neq i$) while $d\bar{p} = 0$: For $i = 1, \dots, n_B$, solve for the sensitivities $\hat{\mathbf{v}}_d^{s(i)}, \hat{p}_d^{(i)}, \hat{e}_d^{(i)}$ from the system

$$\begin{aligned} (a_\square)'(\bullet; \delta\mathbf{v}^s, \hat{\mathbf{v}}_d^{s(i)}) + b_\square(\hat{p}_d^{(i)}, \delta\mathbf{v}^s) \\ = -(a_\square)'(\bullet; \delta\mathbf{v}^s, \hat{\mathbf{v}}_{\text{dev}}^{M(i)}) \quad \forall \delta\mathbf{v}^s \in \mathbb{V}_\square^{(D)}, \end{aligned} \quad (52a)$$

$$b_\square(\delta p, \mathbf{x}_m \hat{e}_d^{(i)} + \hat{\mathbf{v}}_d^{s(i)}) = 0 \quad \forall \delta p \in \mathbb{P}_\square, \quad (52b)$$

$$b_\square(\hat{p}_d^{(i)}, \mathbf{x}_m) \delta \bar{e} = 0 \quad \forall \delta \bar{e} \in \mathbb{R}. \quad (52c)$$

2. $d\bar{p} = 1$ while $d\bar{\mathbf{d}}_{\text{dev}} = \mathbf{0}$: Solve for the sensitivities $\hat{\mathbf{v}}_p^s, \hat{p}_p, \hat{e}_p$ from the system

$$(a_\square)'(\bullet; \delta\mathbf{v}^s, \hat{\mathbf{v}}_p^s) + b_\square(\hat{p}_p, \delta\mathbf{v}^s) = 0 \quad \forall \delta\mathbf{v}^s \in \mathbb{V}_\square^{(D)}, \quad (53a)$$

$$b_\square(\delta p, \mathbf{x}_m \hat{e}_p + \hat{\mathbf{v}}_p^s) = 0 \quad \forall \delta p \in \mathbb{P}_\square, \quad (53b)$$

$$b_\square(\hat{p}_p, \mathbf{x}_m) \delta \bar{e} = -1 \delta \bar{e} \quad \forall \delta \bar{e} \in \mathbb{R}. \quad (53c)$$

4.3. Symmetry properties of the total macroscale tangent

The question arises whether the macroscale tangent problem in (36) is symmetrical. Indeed it can be shown (details in the Appendix) that \mathbf{E}_d has major symmetry, and that $\bar{\mathbf{E}}_p = \bar{\mathbf{C}}_d$. Due to the latter identity, we obtain $\bar{c}'_\nu\{\bullet; \delta\bar{p}, \Delta\bar{\mathbf{v}}\} = \bar{a}'_p\{\bullet; \Delta\bar{\mathbf{v}}, \delta\bar{p}\}$ such that (36) can be rewritten as

$$\begin{aligned} \bar{a}'_\nu\{\bullet; \delta\bar{\mathbf{v}}, \Delta\bar{\mathbf{v}}\} + \bar{a}'_p\{\bullet; \delta\bar{\mathbf{v}}, \Delta\bar{p}\} + \bar{b}\{\Delta\bar{p}, \delta\bar{\mathbf{v}}\} \\ = -\bar{a}\{\bullet; \delta\bar{\mathbf{v}}\} - \bar{b}\{\bullet; \delta\bar{\mathbf{v}}\} \quad \forall \delta\bar{\mathbf{v}} \in \mathbb{V}^0, \end{aligned} \quad (54a)$$

$$\begin{aligned} \bar{b}\{\delta\bar{p}, \Delta\bar{\mathbf{v}}\} + \bar{a}'_p\{\bullet; \Delta\bar{\mathbf{v}}, \delta\bar{p}\} + \bar{c}'_p\{\bullet; \delta\bar{p}, \Delta\bar{p}\} \\ = -\bar{b}\{\delta\bar{p}, \bullet\} - \bar{c}\{\bullet; \delta\bar{p}\} \quad \forall \delta\bar{p} \in \mathbb{P}. \end{aligned} \quad (54b)$$

Remark. Since there is no need to compute $\bar{\mathbf{C}}_d$ as given in (50), there is, in fact, no need to compute the sensitivity fields $\hat{e}_d^{(i)}$; however, these are integral parts of the solution of the sensitivity problems defined by (52). \square

5. Numerical examples

The computations were carried out with a linear constitutive model for the viscous flow. Surface tension was considered only on the particle/pore interface. The viscosity μ and surface energy γ_s were set to unit values, and the time step was adjusted to obtain sufficiently small deformations in each time step.

Two benchmark examples are shown for a single macroscopic material point, where $\bar{\mathbf{d}}_{\text{dev}}, \bar{p}$ (RVE inputs) and $\bar{\boldsymbol{\sigma}}_{\text{dev}}, \bar{e}$ (RVE outputs) are the quantities of interest. This is followed by a complete FE²-simulation.

For the transient part, explicit time integration is used. For each time step, the velocity and pressure are solved instantaneously, and the geometry is updated as; ${}^n \mathbf{x} = {}^{n-1} \mathbf{x} + \Delta t \mathbf{v}$. When the RVE mesh becomes too distorted, it is remeshed.

5.1. Macroscopic shear ($\bar{p} = 0$)

A single unit cell (one pore) is subjected to prescribed constant macroscopic shear rate, i.e., $\bar{\mathbf{d}}_{\text{dev}} \neq \mathbf{0}$, whereas the macroscopic pressure is set to zero, $\bar{p} = 0$. This situation of “mixed control” represents “quasi-free” sintering in the sense that the resulting value of $\bar{\boldsymbol{\sigma}}_{\text{dev}}$ is non-zero (while $\bar{p} = 0$), and it turns out that $\bar{\boldsymbol{\sigma}}_{\text{dev}}$ stays nearly constant throughout the entire simulation time. Snapshots of the evolving RVE-configuration are given in Fig. 5, and it appears that effects of the adopted Dirichlet boundary condition is clearly visible in the severely sheared state.

Vanishing porosity, i.e., macroscopic incompressibility manifested by $\bar{e} = 0$ and $\bar{\phi} = 0$, was reached at around $0.69 t_{\text{end}}$. After this point in time, the deformation continues but is completely isochoric ($\bar{e} = 0$). Artifacts from the remeshing of the RVE are noticeable in Fig. 6 under close examination; however, the overall macroscopic behavior is mostly unaffected.

We remark that, in the adopted mixed macroscale format, $\bar{\mathbf{d}}_{\text{dev}}$ and \bar{p} are the “natural” control variables for the RVE-problems; hence the computation is straight-forward (in contrast to the situation of “free sintering” discussed subsequently).

5.2. Free sintering ($\bar{\boldsymbol{\sigma}} = \mathbf{0}$)

In the next series of RVE-computations, the unit cell was subjected to zero macroscopic stress, i.e., $\bar{\boldsymbol{\sigma}} = \mathbf{0}$. Snapshots of the

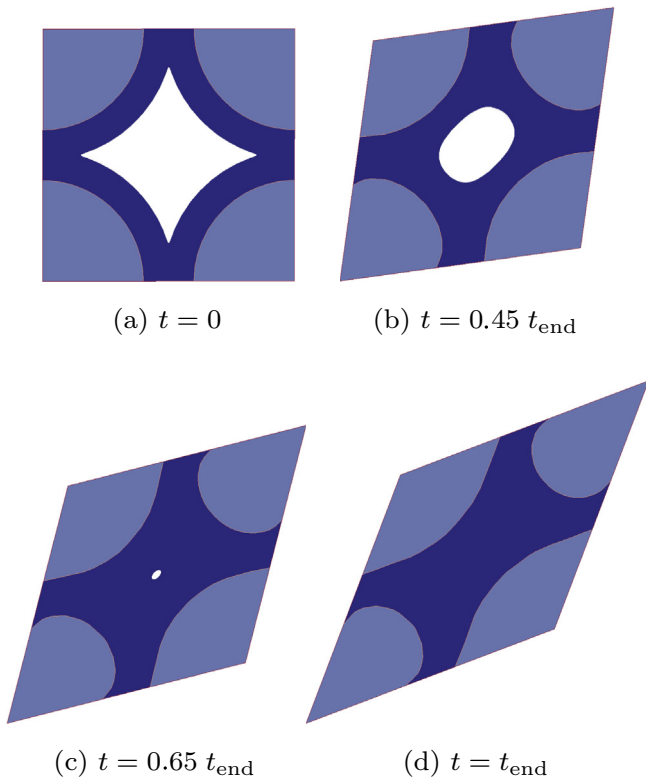


Fig. 5. Snapshots of evolving RVE subjected to constant macroscopic shear rate, $\bar{\mathbf{d}}_{\text{dev}} \neq \mathbf{0}$, and zero macroscopic pressure, $\bar{p} = 0$.

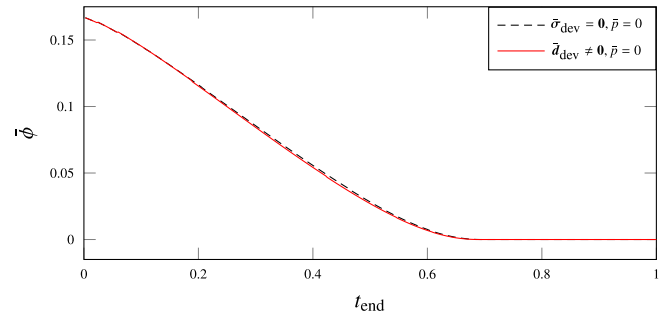


Fig. 6. Evolution of porosity, $\bar{\phi} = 1 - \frac{|\Omega^{\text{part}}|}{|\Omega|}$, with time for the RVE subjected to control representing macroscopic shear ($\bar{\mathbf{d}}_{\text{dev}} \neq \mathbf{0}, \bar{p} = 0$) and free sintering ($\bar{\boldsymbol{\sigma}}_{\text{dev}} = \mathbf{0}, \bar{p} = 0$).

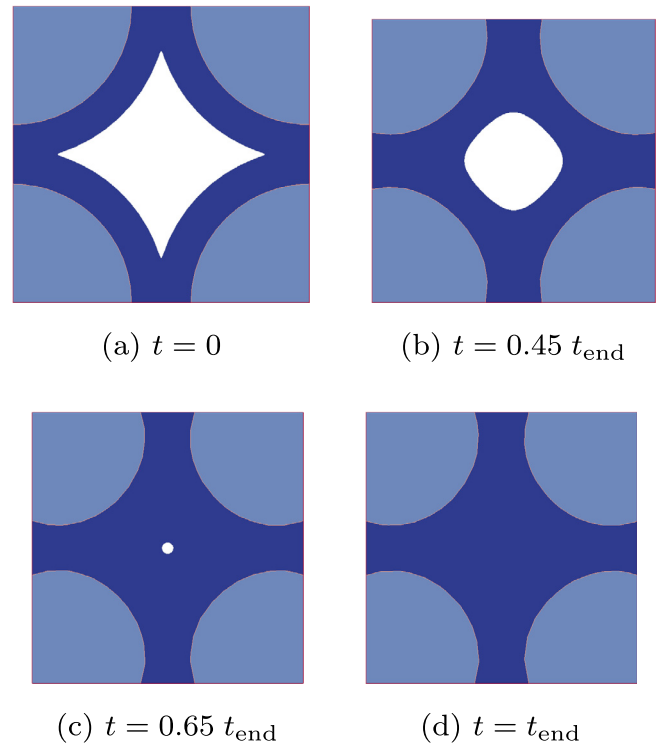


Fig. 7. Snapshots of evolving RVE subjected to zero macroscopic stress, $\bar{\boldsymbol{\sigma}}_{\text{dev}} = \mathbf{0}$ and $\bar{p} = 0$.

evolving RVE-configuration are given in Fig. 7, and the corresponding porosity evolution is shown in Fig. 6. Like in the case of macroscopic shear, a fully dense state was reached at around $0.69 t_{\text{end}}$. However, all deformation stops at this point (which is in contrast to the previously considered case of macroscopic shear).

We remark that prescribing $\bar{\boldsymbol{\sigma}}_{\text{dev}}$ and \bar{p} represents a situation of “stress control” by which macroscale iterations must be carried out on $\bar{\mathbf{d}}_{\text{dev}}$ in order to ensure the prescribed value $\bar{\boldsymbol{\sigma}}_{\text{dev}} = \mathbf{0}$. Hence, the macroscale algorithmic tensors are exploited in the corresponding Newton iterations.

5.3. FE²-simulation

In the last numerical example, we show a fully coupled FE²-simulation, starting from an inhomogeneous initial porosity. Fig. 8 shows how the relative density evolves from the initial state, half-way through, to the fully dense product. The final macroscopic shape distortion is noticeable. In this simulation, 4 integration points are used for every macroscopic element. Zoomed-in on

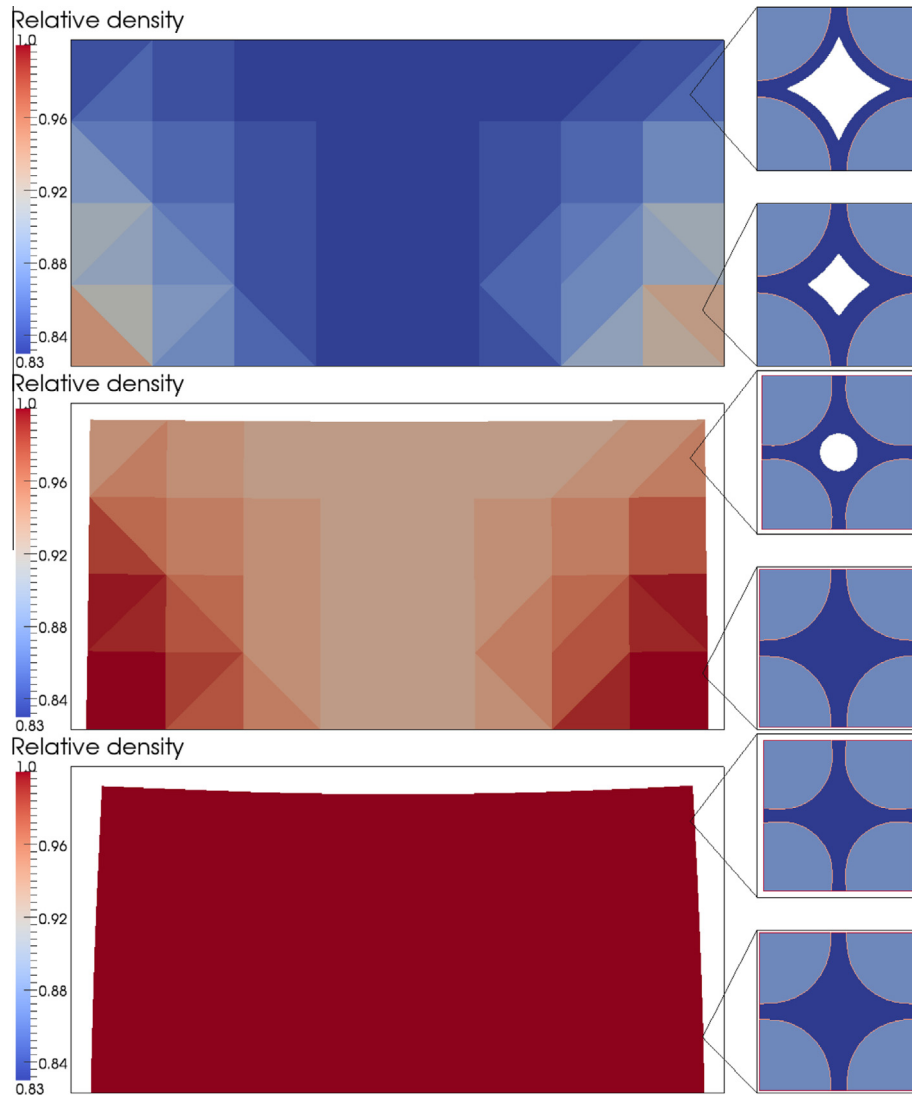


Fig. 8. Snapshots of the macroscopic domain with two selected RVE's throughout the densification process.

the right side of the macroscopic domain, RVEs in two selected integration points are shown. They undergo successive change of both volume and shape (although the shear deformation is hardly noticeable in the Figure).

6. Conclusions and outlook

By introducing the mixed variational $(\bar{\mathbf{v}}, \bar{p})$ -format of the macroscale problem, we can ensure a “seamless” transition from the macroscopically compressible to the incompressible response. Hence, there is no need to change the computational algorithm when the simulation is taken beyond the state of a fully dense macroscopic response (in some spatial point in the macro-domain). Without such a mixed formulation, the macroscopic ATStensor would become unbounded at the transition state. In other words, the “naive” method described in Fig. 3 would break down halfway through the simulation shown in Fig. 8, when any RVE becomes fully dense, while the method in Fig. 4 can continue to a complete dense state without numerical singularities.

The additional variable in the RVE-problem, as compared to the standard format of Stokes’ problem when $\bar{\mathbf{d}}$ is the single variable that represents prolongation from the macroscale to the subscale, is \bar{e} . An additional constraint equation is added to ensure

that the subscale pressure is homogenized to p in a variationally consistent fashion, whereby the test function is $\delta \bar{e} \in \mathbb{R}$. Hence, symmetry is preserved of the linearized RVE-problem due to the variational format of the “Galerkin-type”. The extra computational cost for including \bar{e} is, indeed, very small in the chosen monolithic format.

As an outlook to future developments, the new mixed RVE-format will be adopted in conjunction with micro-periodic and Neumann boundary conditions. It would also be of interest to extend the classical strong format of micro-periodicity to a weak variational setting, cf. Larsson et al. [23]. A major advantage is that the subscale FE-mesh does not need to be periodic, which is particularly beneficial in a context of adaptive mesh (re)generation.

The microstructural properties of the “green body”, i.e., before the sintering process starts, should be represented in a more realistic way than is presently the case. For example, the RVE should be generated from a given statistical distribution of particle size and shape. Parameter variations should be carried out of the various geometrical and constitutive properties. In order to make (inverse) parameter identification meaningful, it is necessary to extend the description of the subscale geometry to three dimensions in the future, although this may represent a major increase in complexity and computational demand.

All code for the simulations shown in the examples is available in the open source finite element code OOFEM at <http://www.oofem.org>.

Appendix A. RVE-problem

The weak format of equilibrium for an RVE is

$$\int_{\Omega_{\square}^{\text{part}}} \boldsymbol{\sigma} : [\delta \mathbf{v} \otimes \nabla] d\mathbf{v} = \int_{\Gamma_{\square} \cup \Gamma_{\square}^{\text{pore}}} \mathbf{t} \cdot \delta \mathbf{v} da \quad (\text{A.1})$$

for suitable choice of test functions $\delta \mathbf{v}$. Testing (A.1) with $\delta \mathbf{v}^s$, we directly obtain

$$\int_{\Omega_{\square}^{\text{part}}} \boldsymbol{\sigma} : [\delta \mathbf{v}^s \otimes \nabla] d\mathbf{v} = \int_{\Gamma_{\square}^{\text{pore}}} \mathbf{t}_s \cdot \delta \mathbf{v}^s da \quad (\text{A.2})$$

which is precisely (22a). Next, testing (A.1) with $\mathbf{v}_{\text{vol}}^M(\delta \bar{\mathbf{e}})$, we obtain

$$-\left[\int_{\Omega_{\square}^{\text{part}}} p d\mathbf{v} \right] \delta \bar{\mathbf{e}} = \left[\int_{\Gamma_{\square}^{\text{pore}}} \mathbf{t}_s \cdot \mathbf{x}_m da \right] \delta \bar{\mathbf{e}} - |\Omega_{\square}| \bar{p} \delta \bar{\mathbf{e}}, \quad (\text{A.3})$$

where it was used that $[\mathbf{x}_m \otimes \nabla] = \frac{1}{3} \mathbf{I}$, $p = -\frac{1}{3} \mathbf{I} : \boldsymbol{\sigma}$ and

$$\bar{p} = -\frac{1}{|\Omega_{\square}|} \int_{\Gamma_{\square}} \mathbf{t} \cdot \mathbf{x}_m da = -\underbrace{\left[\frac{1}{|\Omega_{\square}|} \int_{\Gamma_{\square}} \mathbf{t} \otimes [\mathbf{x} - \bar{\mathbf{x}}] da \right]}_{\boldsymbol{\sigma}} : \frac{1}{3} \mathbf{I}. \quad (\text{A.4})$$

Dividing (A.3) by $|\Omega_{\square}|$, we obtain (22c).

Appendix B. Base dyadics in sensitivity problem

The orthonormal base \mathbf{E}_i can be chosen in a cartesian basis, in 2D, as

$$\mathbf{E}_1 = \frac{1}{\sqrt{2}} \begin{bmatrix} 1 & 0 \\ 0 & -1 \end{bmatrix}, \quad \mathbf{E}_2 = \frac{1}{\sqrt{2}} \begin{bmatrix} 0 & 1 \\ 1 & 0 \end{bmatrix} \quad (\text{B.1})$$

and in 3D, as

$$\begin{aligned} \mathbf{E}_1 &= \frac{1}{\sqrt{6}} \begin{bmatrix} 2 & 0 & 0 \\ 0 & -1 & 0 \\ 0 & 0 & -1 \end{bmatrix}, & \mathbf{E}_2 &= \frac{1}{\sqrt{2}} \begin{bmatrix} 0 & 0 & 0 \\ 0 & 1 & 0 \\ 0 & 0 & -1 \end{bmatrix}, \\ \mathbf{E}_3 &= \frac{1}{\sqrt{2}} \begin{bmatrix} 0 & 1 & 0 \\ 1 & 0 & 0 \\ 0 & 0 & 0 \end{bmatrix}, & \mathbf{E}_4 &= \frac{1}{\sqrt{2}} \begin{bmatrix} 0 & 0 & 1 \\ 0 & 0 & 0 \\ 1 & 0 & 0 \end{bmatrix}, \\ \mathbf{E}_5 &= \frac{1}{\sqrt{2}} \begin{bmatrix} 0 & 0 & 0 \\ 0 & 0 & 1 \\ 0 & 1 & 0 \end{bmatrix}. \end{aligned} \quad (\text{B.2})$$

Appendix C. Symmetry of the macro-scale problem

In order to prove symmetry of the macroscale tangent problem it is sufficient to show that it is possible to construct a potential $\bar{\Pi}\{\bar{\mathbf{d}}_{\text{dev}}, \bar{p}\}$ with the properties

$$\frac{\partial \bar{\Pi}}{\partial \bar{\mathbf{d}}_{\text{dev}}} = \bar{\boldsymbol{\sigma}}_{\text{dev}}, \quad \frac{\partial \bar{\Pi}}{\partial \bar{p}} = \bar{e} \quad (\text{C.1})$$

from which it follows directly that

$$\bar{\mathbf{E}}_{\text{d}} \stackrel{\text{def}}{=} \frac{\partial \bar{\boldsymbol{\sigma}}_{\text{dev}}}{\partial \bar{\mathbf{d}}_{\text{dev}}} = \frac{\partial^2 \bar{\Pi}}{\partial \bar{\mathbf{d}}_{\text{dev}} \otimes \partial \bar{\mathbf{d}}_{\text{dev}}} \quad (\text{C.2})$$

and

$$\bar{\mathbf{E}}_{\text{p}} = \frac{\partial \bar{\boldsymbol{\sigma}}_{\text{dev}}}{\partial \bar{p}} = \frac{\partial^2 \bar{\Pi}}{\partial \bar{\mathbf{d}}_{\text{dev}} \partial \bar{p}} = \frac{\partial \bar{e}}{\partial \bar{\mathbf{d}}_{\text{dev}}} \stackrel{\text{def}}{=} \bar{\mathbf{C}}_{\text{d}}. \quad (\text{C.3})$$

We note that that the “tangent stiffness” tensor $\bar{\mathbf{E}}_{\text{d}}$ is symmetrical.

In order to show (C.1), we start by assuming that it is possible to establish the subscale potential $\Pi_{\square}(\bar{\mathbf{d}}_{\text{dev}}, \bar{p}; \mathbf{v}^s, p, \bar{\mathbf{e}})$, for given macroscale values $\bar{\mathbf{d}}_{\text{dev}}, \bar{p}$, such that the RVE-problem in (22) can be stated as

$$\Pi'_{\square, \mathbf{v}^s}(\bullet; \delta \mathbf{v}^s, p, \bar{\mathbf{e}}) = 0 \quad \forall \delta \mathbf{v}^s \in \mathbb{V}_{\square}^{(\text{D})}, \quad (\text{C.4a})$$

$$\Pi'_{\square, p^s}(\bullet; \mathbf{v}^s, \delta p, \bar{\mathbf{e}}) = 0 \quad \forall \delta p \in \mathbb{P}_{\square}, \quad (\text{C.4b})$$

$$\Pi'_{\square, \bar{\mathbf{e}}}(\bullet; \mathbf{v}^s, p, \delta \bar{\mathbf{e}}) = 0 \quad \forall \delta \bar{\mathbf{e}} \in \mathbb{R}. \quad (\text{C.4c})$$

More explicitly, we define

$$\Pi_{\square}(\bar{\mathbf{d}}_{\text{dev}}, \bar{p}, \mathbf{v}^s, p, \bar{\mathbf{e}}) = \Psi_{\square}(\mathbf{v}) + b_{\square}(p, \mathbf{v}) - l_{\square}^{\text{pore}}(\mathbf{v}) + \bar{p} \bar{\mathbf{e}}, \quad (\text{C.5})$$

where we introduced the subscale free energy $\Psi_{\square}(\mathbf{v})$ such that

$$\Psi'_{\square}(\mathbf{v}; \delta \mathbf{v}) = a_{\square}(\mathbf{v}; \delta \mathbf{v}) \quad (\text{C.6})$$

and used tacitly the parametrization of the velocity

$$\mathbf{v} = \mathbf{v}(\bar{\mathbf{d}}_{\text{dev}}, \bar{\mathbf{e}}, \mathbf{v}^s) = \bar{\mathbf{d}}_{\text{dev}} \cdot [\mathbf{x} - \bar{\mathbf{x}}] + \bar{\mathbf{e}} \mathbf{x}_m + \mathbf{v}^s. \quad (\text{C.7})$$

It thus follows trivially that (C.4) is precisely the RVE-problem stated in (22).

Now, let us define the macroscale potential $\bar{\Pi}$ as follows

$$\bar{\Pi}\{\bar{\mathbf{d}}_{\text{dev}}, \bar{p}\} \stackrel{\text{def}}{=} \Pi_{\square}(\bar{\mathbf{d}}_{\text{dev}}, \bar{p}, \mathbf{v}^s\{\bar{\mathbf{d}}_{\text{dev}}, \bar{p}\}, p\{\bar{\mathbf{d}}_{\text{dev}}, \bar{p}\}, \bar{\mathbf{e}}\{\bar{\mathbf{d}}_{\text{dev}}, \bar{p}\}), \quad (\text{C.8})$$

where we tacitly account for the implicit relations $\mathbf{v}^s\{\bar{\mathbf{d}}_{\text{dev}}, \bar{p}\}$, $p^s\{\bar{\mathbf{d}}_{\text{dev}}, \bar{p}\}$, and $\bar{\mathbf{e}}\{\bar{\mathbf{d}}_{\text{dev}}, \bar{p}\}$ via the solution of the RVE-problem (C.4) for given values of (the macroscale variables) $\bar{\mathbf{d}}_{\text{dev}}$ and \bar{p} . Using the chain rule of differentiation and using (C.4), we then obtain the identities

$$\frac{\partial \bar{\Pi}}{\partial \bar{\mathbf{d}}_{\text{dev}}} = \frac{\partial \Pi_{\square}}{\partial \bar{\mathbf{d}}_{\text{dev}}}\bigg|_{\bar{p}, \mathbf{v}^s, p, \bar{\mathbf{e}}}, \quad \frac{\partial \bar{\Pi}}{\partial \bar{p}} = \frac{\partial \Pi_{\square}}{\partial \bar{p}}\bigg|_{\bar{\mathbf{d}}_{\text{dev}}, \mathbf{v}^s, p, \bar{\mathbf{e}}}. \quad (\text{C.9})$$

However, from the construction of the functional Π_{\square} in (C.5), we obtain

$$\begin{aligned} \frac{\partial \Pi_{\square}}{\partial \bar{\mathbf{d}}_{\text{dev}}} : \text{d}\bar{\mathbf{d}}_{\text{dev}} &= a_{\square}(\mathbf{v}; \text{d}\bar{\mathbf{d}}_{\text{dev}} \cdot [\mathbf{x} - \bar{\mathbf{x}}]) \\ &+ \underbrace{b_{\square}(\text{d}\bar{\mathbf{d}}_{\text{dev}} \cdot [\mathbf{x} - \bar{\mathbf{x}}])}_{=0} - l_{\square}^{\text{pore}}(\text{d}\bar{\mathbf{d}}_{\text{dev}} \cdot [\mathbf{x} - \bar{\mathbf{x}}]), \end{aligned} \quad (\text{C.10a})$$

$$\frac{\partial \Pi_{\square}}{\partial \bar{p}} \text{d}\bar{p} = \bar{e} \text{d}\bar{p} \quad (\text{C.10b})$$

and with (41) we obtain

$$a_{\square}(\mathbf{v}; \text{d}\bar{\mathbf{d}}_{\text{dev}} \cdot [\mathbf{x} - \bar{\mathbf{x}}]) = \sum_{i=1}^{n_{\text{B}}} a_{\square}(\mathbf{v}; \mathbf{E}_i \cdot [\mathbf{x} - \bar{\mathbf{x}}]) \mathbf{E}_i : \text{d}\bar{\mathbf{d}}_{\text{dev}}, \quad (\text{C.11})$$

$$l_{\square}^{\text{pore}}(\text{d}\bar{\mathbf{d}}_{\text{dev}} \cdot [\mathbf{x} - \bar{\mathbf{x}}]) = \sum_{i=1}^{n_{\text{B}}} l_{\square}^{\text{pore}}(\mathbf{E}_i \cdot [\mathbf{x} - \bar{\mathbf{x}}]) \mathbf{E}_i : \text{d}\bar{\mathbf{d}}_{\text{dev}}. \quad (\text{C.12})$$

Next, we can combine (42) with (24) to obtain

$$\bar{\boldsymbol{\sigma}}_{\text{dev}} = \sum_{i=1}^{n_{\text{B}}} [a_{\square}(\mathbf{v}; \mathbf{E}_i \cdot [\mathbf{x} - \bar{\mathbf{x}}]) - l_{\square}^{\text{pore}}(\mathbf{E}_i \cdot [\mathbf{x} - \bar{\mathbf{x}}])] \mathbf{E}_i \quad (\text{C.13})$$

and combining this result with (C.11) and (C.12), we may rephrase (C.9) as

$$\frac{\partial \Pi_{\square}}{\partial \bar{\mathbf{d}}_{\text{dev}}}\bigg|_{\bar{p}, \mathbf{v}^s, p, \bar{\mathbf{e}}} = \bar{\boldsymbol{\sigma}}_{\text{dev}} : \text{d}\bar{\mathbf{d}}_{\text{dev}}. \quad (\text{C.14})$$

Finally, combining (C.14) and (C.10b) with (C.9), we obtain the desired properties in (C.1). Hence, symmetry is proven.

References

- [1] A. Jagota, P.R. Dawson, Micromechanical modeling of powder compacts I. Unit problems for sintering and traction induced deformation, *Acta Metall.* 36 (9) (1988) 2551–2561. <<http://linkinghub.elsevier.com/retrieve/pii/S001616088902003>>.
- [2] A. Jagota, P.R. Dawson, Micromechanical modeling of powder compacts II. Truss formulation of discrete packings, *Acta Metall.* 36 (9) (1988) 2563–2573, [http://dx.doi.org/10.1016/0001-6160\(88\)90201-5](http://dx.doi.org/10.1016/0001-6160(88)90201-5).
- [3] G.A.L. van de Vorst, Integral method for a two-dimensional Stokes flow with shrinking holes applied to viscous sintering, *J. Fluid Mech.* 257 (1993) 667–689, <http://dx.doi.org/10.1017/S002211209300326X>.
- [4] H. Zhou, J.J. Derby, Three-dimensional finite-element analysis of viscous sintering, *J. Am. Ceram. Soc.* 81 (3) (1998) 533–540, <http://dx.doi.org/10.1111/j.1151-2916.1998.tb02371.x>.
- [5] H. Zhou, J.J. Derby, An assessment of a parallel finite element method for three-dimensional moving-boundary flows driven by capillarity for simulation of viscous sintering, *Int. J. Numer. Methods Fluids* 36 (7) (2001) 841–865, <http://dx.doi.org/10.1002/flid.159>.
- [6] W.G. Dettmer, D. Perić, A computational framework for free surface fluid flows accounting for surface tension, *Comput. Methods Appl. Mech. Eng.* 195 (23–24) (2006) 3038–3071, <http://dx.doi.org/10.1016/j.cma.2004.07.057>.
- [7] P.H. Saksono, D. Perić, On finite element modelling of surface tension: variational formulation and applications. Part I: Quasistatic problems, *Comput. Mech.* 38 (3) (2006) 265–281. <<http://www.springerlink.com/index/10.1007/s00466-005-0747-5>>.
- [8] P.H. Saksono, D. Perić, On finite element modelling of surface tension: variational formulation and applications. Part II: Dynamic problems, *Comput. Mech.* 38 (3) (2006) 251–263, <http://dx.doi.org/10.1007/s00466-005-0745-7>.
- [9] A. Javili, P. Steinmann, A finite element framework for continua with boundary energies. Part I: The two-dimensional case, *Comput. Methods Appl. Mech. Eng.* 198 (27–29) (2009) 2198–2208. <<http://linkinghub.elsevier.com/retrieve/pii/S0045782509000802>>.
- [10] A. Javili, P. Steinmann, A finite element framework for continua with boundary energies. Part II: The three-dimensional case, *Comput. Methods Appl. Mech. Eng.* 199 (9–12) (2010) 755–765, <http://dx.doi.org/10.1016/j.cma.2009.11.003>.
- [11] C.R. Reid, R.G. Oakberg, A continuum theory for the mechanical response of materials to the thermodynamic stress of sintering, *Mech. Mater.* 10 (3) (1990) 203–213, [http://dx.doi.org/10.1016/0167-6636\(90\)90043-F](http://dx.doi.org/10.1016/0167-6636(90)90043-F).
- [12] L. Mähler, K. Runesson, Modelling of solid-phase sintering of hardmetal using a mesomechanics approach, *Mech. Cohesive-frictional Mater.* 5 (8) (2000) 653–671. <[http://doi.wiley.com/10.1002/1099-1484\(200011\)5:8653:AID-CFM113.0.CO;2-A](http://doi.wiley.com/10.1002/1099-1484(200011)5:8653:AID-CFM113.0.CO;2-A)>.
- [13] J. Svoboda, H. Riedel, R. Gaebel, A model for liquid phase sintering, *Acta Mater.* 44 (8) (1996) 3215–3226. <<http://linkinghub.elsevier.com/retrieve/pii/S1359645495004408>>.
- [14] K. Xu, M.M. Mehrabadi, A micromechanical model for the initial rearrangement stage of liquid phase sintering, *Mech. Mater.* 25 (2) (1997) 137–157. <[http://dx.doi.org/10.1016/S0167-6636\(96\)00048-8](http://dx.doi.org/10.1016/S0167-6636(96)00048-8)>.
- [15] P. Lu, W. Yi, X. Xu, R.M. German, Porosity effect on densification and shape distortion in liquid phase sintering, *Mater. Sci. Eng. A* 318 (1–2) (2001) 111–121. <[http://dx.doi.org/10.1016/S0921-5093\(01\)01330-2](http://dx.doi.org/10.1016/S0921-5093(01)01330-2)>.
- [16] C. Sandström, F. Larsson, Variationally consistent homogenization of Stokes flow in porous media, *Int. J. Multiscale Comput. Eng.* 11 (2) (2013), <http://dx.doi.org/10.1615/IntJMultCompEng.2012004069>.
- [17] T.I. Zohdi, P. Wriggers, A model for simulating the deterioration of structural-scale material responses of microheterogeneous solids, *Comput. Methods Appl. Mech. Eng.* 190 (22–23) (2001) 2803–2823. <<http://linkinghub.elsevier.com/retrieve/pii/S0045782500003674>>.
- [18] S. Klinge, K. Hackl, Application of the multiscale FEM to the modeling of nonlinear composites with a random microstructure, *Int. J. Multiscale Comput. Eng.* 10 (3) (2012) 213–227. <<http://www.begellhouse.com/journals/61fd1b191cf7e96f.20e1ba4b4b9313c6.08eb49da2ef0c980.html>>.
- [19] C. Miehe, J. Schröder, J. Schotte, Computational homogenization analysis in finite plasticity Simulation of texture development in polycrystalline materials, *Comput. Methods Appl. Mech. Eng.* 171 (3–4) (1999) 387–418. <<http://linkinghub.elsevier.com/retrieve/pii/S0045782598002187>>.
- [20] C. Oskay, J. Fish, Eigen deformation-based reduced order homogenization for failure analysis of heterogeneous materials, *Comput. Methods Appl. Mech. Eng.* 196 (7) (2007) 1216–1243. <<http://linkinghub.elsevier.com/retrieve/pii/S0045782506002933>>.
- [21] M. Öhman, K. Runesson, F. Larsson, Computational mesoscale modeling and homogenization of liquid-phase sintering of particle agglomerates, *Tech. Mech.* 32 (2012) 463–483. <<http://www.uni-magdeburg.de/ifme/zeitschrift/2012Heft25/33Oehman.pdf>>.
- [22] P. Steinmann, On boundary potential energies in deformational and configurational mechanics, *J. Mech. Phys. Solids* 56 (3) (2008) 772–800, <http://dx.doi.org/10.1016/j.jmps.2007.07.001>.
- [23] F. Larsson, K. Runesson, S. Saroukhani, R. Vafadari, Computational homogenization based on a weak format of micro-periodicity for RVE-problems, *Comput. Methods Appl. Mech. Eng.* 200 (1–4) (2011) 11–26. <<http://linkinghub.elsevier.com/retrieve/pii/S0045782510001908>>.